TOWARDS THE LIMITS IN COPPER LATTICE PRODUCTION VIA FIBER LASER POWDER BED FUSION

M. Smet*, G. Li†, L.R. Goossens*, S. Buls*, B. Van Hooreweder*

*Department of Mechanical Engineering, KU Leuven, Belgium,
†Department of Materials Engineering, KU Leuven, Belgium

Abstract

Additive manufacturing of copper, by means of Laser Powder Bed Fusion (LPBF), paves the way for innovation in thermal systems and heat transfer devices. Recent simulations have shown that by interchanging typical fin designs with more complex structures, an overall improvement in pressure drop and weight can be obtained while offering the same thermal performance. Here, small-scale lattice structures are especially of interest for AM as they form a reliable, periodic infill. However, until now, their study has been mainly theoretical. To analyze these structures in more detail, an in-house built LPBF machine at KU Leuven has been successfully used to manufacture pure copper parts. Measurements showed a conductivity exceeding 100%IACS, which is the result of low contamination and low porosity in the as-built material. In this work, the parameter optimization for thin-walled lattices is discussed, the limitations in terms of minimal feature size are described and physical mechanisms behind these limitations are uncovered.

1. **Introduction**

Pure Cu has been proven to be difficult to produce by additive manufacturing (AM) due to its high reflectivity at infrared laser wavelengths and high thermal conductivity. Even so, many researchers have taken on this challenge. Distinction can be made between direct and indirect additive manufacturing techniques. Indirect methods make use of a binder material, typically a polymer, to avoid the common challenges of pure copper AM. However, after removing the binder material, impurities are left in the copper and will deteriorate the thermal properties (93.3 %IACS) and mechanical properties (80.2% wrought strength). [1] This often makes direct AM the preferred technique when high conductivity is required. Among direct AM techniques (i.e. Powder/Wire DED, EBM, LS, LPBF) , shown in table 1, LPBF shows the highest potential when dense (>99.5%), highly conductive (>99 %IACS), complex shaped (fine features < 250µm) and relatively smooth (Ra < 10µm) pure copper parts are envisioned. [2], [3], [4].

REF	Technique	Power source	Density [%]	IACS [%]	Layer [µm]	Hatch [µm]	Power [W]	Speed [mm/s]
[1]	Binder Jetting	/	97.3	94.5	70	/	/	/
[2]	EBM	Electron beam	99.9	100	50	/	1200	3000
[3]	LPBF	Fiber laser	99.6	76.1	10	50	200	600
[4]	LPBF	Fiber laser	99.3	94	30	90	500	800

Table 1: Overview of some published copper-AM techniques

LPBF of pure copper at fiber-laser wavelength of 1064nm is challenging but has recently been shown as an effective method in building dense copper parts using commercially available LPBF equipment. [4] Even though the processing window is very small, densities up to 99.7% can be achieved consistently at scanning speed of 800±50 mm/s, laser power of 550±100W, hatch spacing of 100µm and layer thickness 30µm. Processing copper this way has been a major challenge as a result of the high thermal conductivity and high reflectivity of pure copper at fiber-laser wavelength. This is why pure copper is being processed in keyhole mode rather than conduction mode. The keyhole melt pool, as shown in Figure 1, allows for better absorption of the laser-light via multiple internal reflections effectively creating a stable LPBF-process.
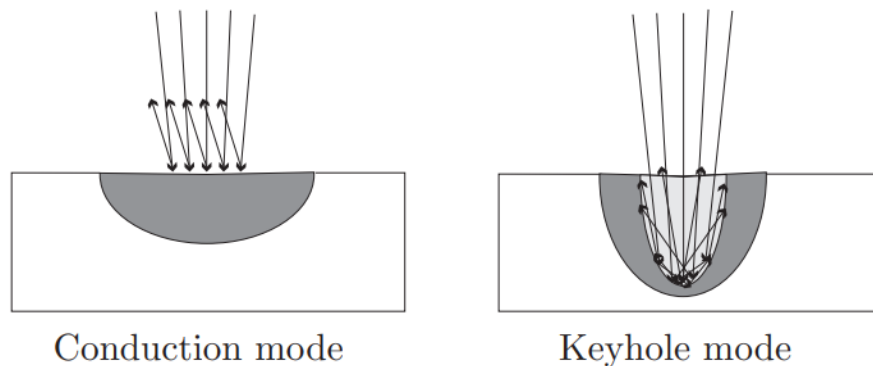

Figure 1: Conduction melt pool vs. keyhole melt pool [5]

Processing in keyhole mode implies that the melt pool is deep compared to a conduction mode melt pool. Although this typically does not form a problem for bulk parts, it becomes a limiting factor for the precision and minimum feature size when building inclined and overhanging struts or surfaces for lattice structures. This paper discusses the effect of the keyhole melt pool mode in Cu-LPBF on the precision and general properties of lattice structures produced by standard LPBF equipment.

2. Machine, process and measurements

The data discussed in this paper were obtained using the in-house developed LPBF-machine (LM-Q) in the Additive Manufacturing Lab at KU Leuven. The LM-Q is equipped with a 1 kW nLight fiber laser with 1064nm wavelength and 37.5µm spotsize combined with a modified optical train to cope with back reflections. Samples in this study were built using atomized OF-Cu powder (10-80µm) provided by Safina. Laser Power P, scan speed v and baseplate preheating were varied to determine optimal process parameters for both bulk and small scale samples. Other process parameters such as layer thickness and hatch distance were kept constant at 30µm and 100µm respectively. The LPBF process took place in an inert argon atmosphere (<10ppm O_2) with a slight overpressure of 100mbar.

The quality of the as-built samples was quantified using several measurement methods. The relative density of bulk samples was determined based on the Archimedes principle. However, due to the inherent inibility to measure "open porosity"[1], this Archimedes' measurements are less accurate for thin-walled and strut-based structures. Instead, cross-sections were analyzed by optical microscopy to visualize and locate porosities.

To get a better understanding of the geometrical limitations imposed by the production process, an effort was made to visualize the meltpools. A combination of polishing (up to 1µm) and electrochemical etching (40% H_3PO_4 electrolyte, 0.5VDC, 30-45s) proved to be the most effective method. Images presented in the paper were made using Scanning Electron Microscopy (SEM) and Keyence optical microscopy (OM).

3. Bulk material optimization

Fiber-LPBF of OF-Cu at 1064nm is characterized by a small processing window as keyhole formation is essential for a stable process. When keyhole formation is not achieved, the as-built part will contain lack-of-fusion porosity as a result of insufficient laser absorption. On the other hand, when the energy density is too high, keyhole porosities can occur. This section covers the effect of baseplate preheating on process stability and meltpool formation.

3.1. Baseplate preheating

Amongst others, Tolochko et al. noted that the baseplate temperature has a significant impact on laser absorptivity. [6] Additionally, a higher baseplate temperature results in a smaller temperature difference to reach a molten copper phase. As a result, one can expect a dependency of the optimal process parameters on the baseplate temperature.

The effect of preheating was quantified in this work by three buildjobs (no preheating, 200°C, and 300°C preheating) of each 35 vertical bars with cross-section 5×5mm² and height 40mm. The relative density of the bars was measured using the Archimedes principle. Figure 2.b presents these data in the form of regression models ($R^2 = 0.989$) for the three preheating conditions. The observed maximum relative density (RD) for all three conditions is roughly the same around 99.7% but can be found at slightly different process parameters as shown in Table 2. As expected, a lower energy density (i.e. lower power and higher scan speed) is required at higher baseplate temperatures.

The main effect of preheating is observed in the process stability. In case no preheating is used, the baseplate will naturally reach a temperature of around 250°C after several printing hours. As discussed, this temperature change causes a shift in optimal process parameters, meaning that the process window becomes even smaller. Projections in the x,y-plane in Figure 2.b show the area where the relative density exceeds 99.5% for the three cases. It is clear that by eliminating this temperature change, a wider processing window is obtained.

---

1. Open porosity is a collection of pores that are only partially trapped in a part and therefore connected to the outside surface. When submerging the part in ethanol, those pores are filled and therefore excluded from the Archimedes measurement.
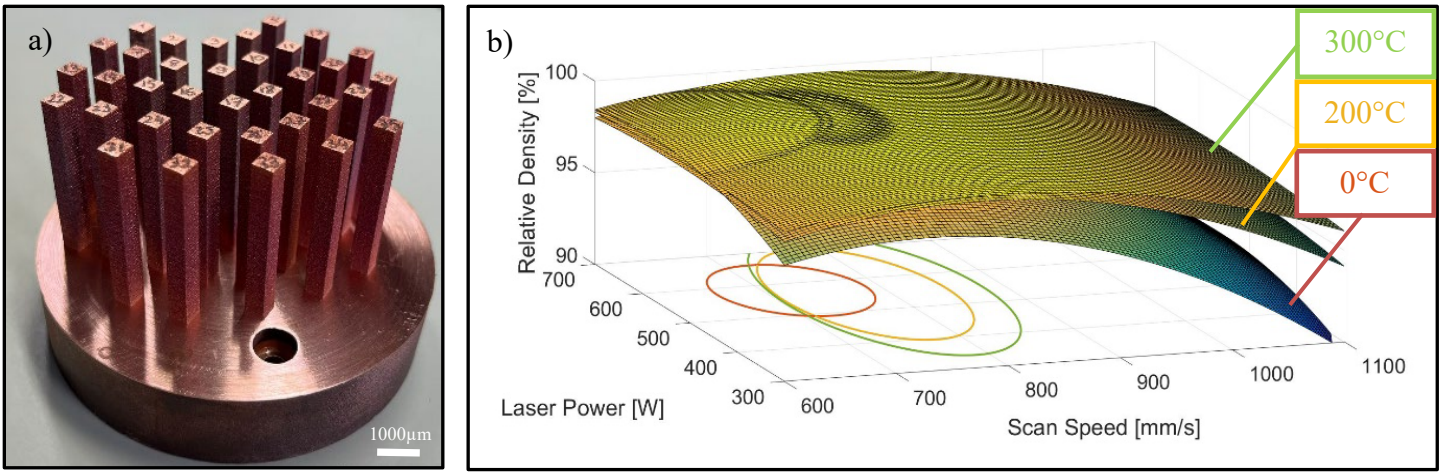
Figure 2: a) As-built bar samples (5×5×40 mm³), b) Regression models of the measured density in function of laser power and scan speed for 0°C, 200°C and 300°C preheating and projection on the x,y-plane showing the +99.5% process window for the three preheating conditions.

Optimal parameter sets	RD [%]	Power [W]	Scan Speed [mm/s]	P/v [J/mm]	Regression equation
0°C	99.74	575	725	0.793	ρ_0°C = 58.642 + 0.038636P + 0.082788v - (2.4e-06) Pv - 3.1959e-05P² - 5.6267e-05v²;
200°C	99.75	550	780	0.705	ρ_200°C = 68.18 + 0.011232P + 0.073255v + (6.5714e-07) Pv - (1.0694e-05) P² - 4.7324e-05v²;
300°C	99.78	540	790	0.684	ρ_300°C = 76.776 + 0.0064554P + 0.053671v + (1.0714e-06) Pv - 6.7347e-06P² - 3.4257e-05v²

Table 2: Optimal process parameters obtained from the regression models shown in Figure 2.

The electrical conductivity of the manufactured bars is measured using a 4-point contact method on a Resistomat® machine (model 2301-V001 of Burster) . For the high density bars, the conductivity was found to consistently exceed 100%IACS which indicates a very low amount of impurities in the as-built condition.

3.2. Bulk melt pool analysis

Melt pool dimensions are expected to be the main limiting factor on the LPBF-process minimum feature size. This section discusses the performed experimental study to assess the effect of power P and scan speed v on the size of the melt pool.

Visualization of melt pool boundaries (MPB) usually relies on distinctive microstructural features, like precipitates or micro-segregation [7], that form near the MPB as a result of rapid solidification. Because OF-Cu is a pure metal and thereby has no alloying elements that can form similar features, visualization of MPB becomes very difficult. Therefore, the fact that dislocations are formed in the crystal structure near the MPB is exploited for MPB visualization. Electrochemical etching will preferentially attack high energy sites, first grain boundaries (GB) and then dislocations, as can be seen in Figure 3.a. A close-up of the MPB, shown in Figure 3.b, reveals the actual size (≈1μm) and morphology of the etched MPB.
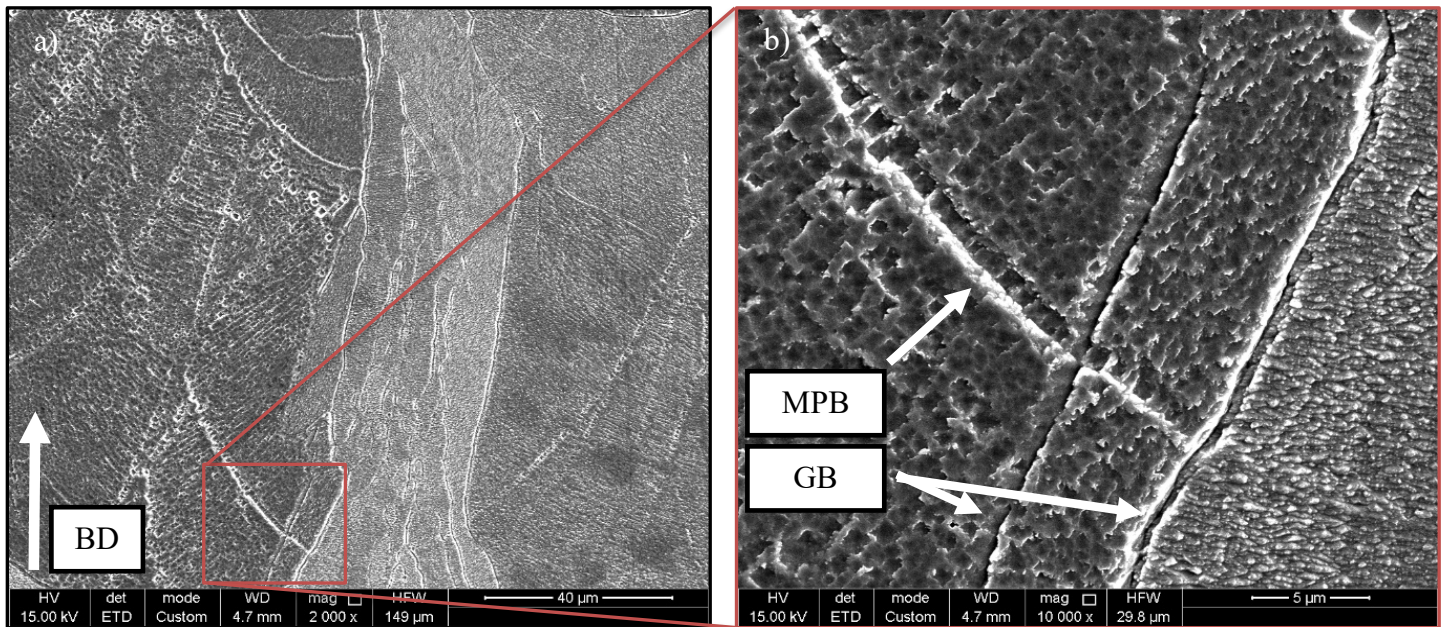
Figure 3: a) SEM-image of the grain and melt pool boundaries after electrochemical etching with 40% H_3PO_4 at 0.5VDC for 45s. b) Close-up image of the MPB.

The solid lines in Figure 4 show the experimentally determined melt pool depth for an applied laser power (300W < P < 600W) and scan speed (200mm/s < v < 1200mm/s) at 300°C baseplate preheating. The graphs indicate a strong relation between melt pool depth and laser power P and scan speed v. The melt pool depth stabilizes at both low (<400mm/s) and high (>1000mm/s) scan speed. In between, a transition from a shallow to a deep melt pool is observed that can be linked to the transition from conduction to keyhole mode. The process parameters referring to the data point in this transitional regime (v = 800mm/s & 400W < P < 600W) fall within the 99.5% process window found in section 1.1., confirming the claim that OF-Cu LPBF is best processed near the keyhole regime. The dashed lines in Figure 4.b refer to the results found by Suraj et al. [4] for OF-LPBF without baseplate preheating. In this scenario, it is probable that the slightly smaller depths reported can be explained by the lower baseplate temperature.
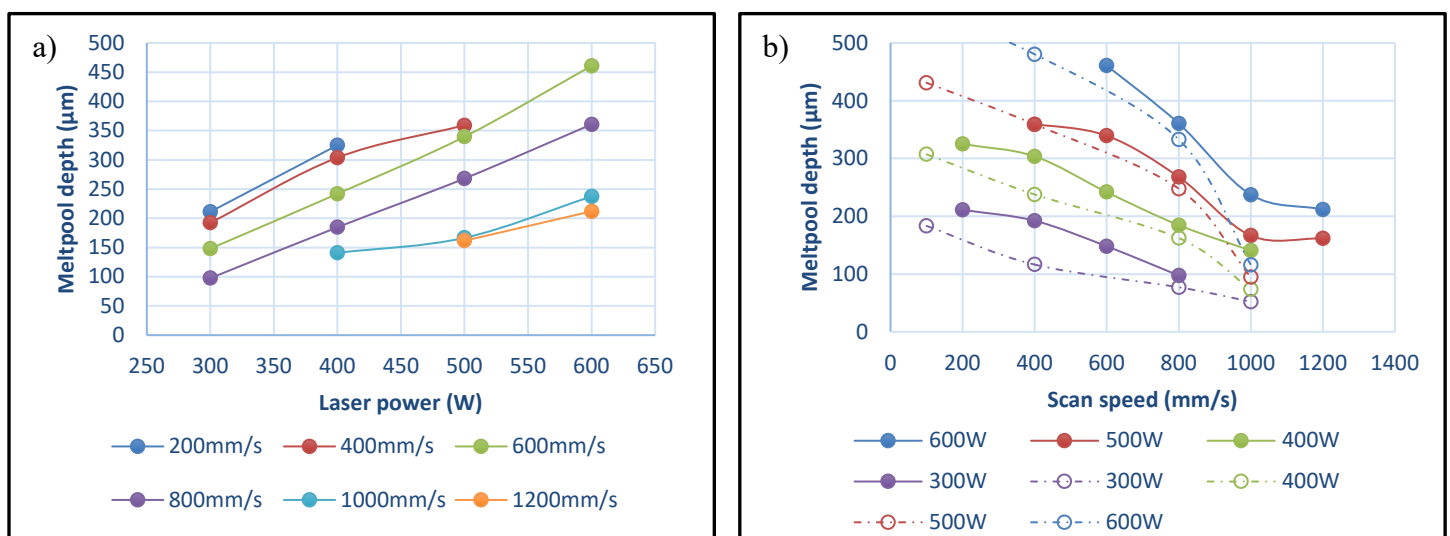

Figure 4: Melt pool depth measured at 300°C baseplate preheating in function of a) Laser power P and b) Scan speed v.

4. <u>Thin wall optimization</u>

Due to the complexity of the LPBF process, it is expected that melt pool formation and melt pool size in bulk material might not be representative for the production of strut- or surface-based lattices. This section covers the melt pool behavior in vertical thin wall structures manufactured by stacking single scan tracks. A large range of process parameters was used to map a process window and study defects present in the samples.

4.1. Parameter optimization

Due to the limited weight and presence of open porosity in these single wall samples, density measurements based on Archimedes' principle may not accurately represent the true density. Therefore, the optimization is based on polished cross-sections. A representative etched cross-section of a single wall is shown in Figure 5. Here the lack of pores, the stable straight shape and the acceptable roughness is clearly visible.

When analyzing cross-sections of the thin walls, a similar process window can be created as for bulk-LPBF. At high power and high speed, the melt pool becomes unstable, leading to balling and a lot of spatter formation. At high Line Energy Density (LED) values, the keyhole melt pool becomes wider and deeper and keyhole porosity is more likely to occur. At low LED-values, on the other hand, the keyhole melt pool cannot be formed properly. As not enough energy can be absorbed, powder will only be sintered together resulting in lack of fusion throughout the part. Figure 6 gives an overview of the different defects found in thin-wall production using suboptimal parameters.
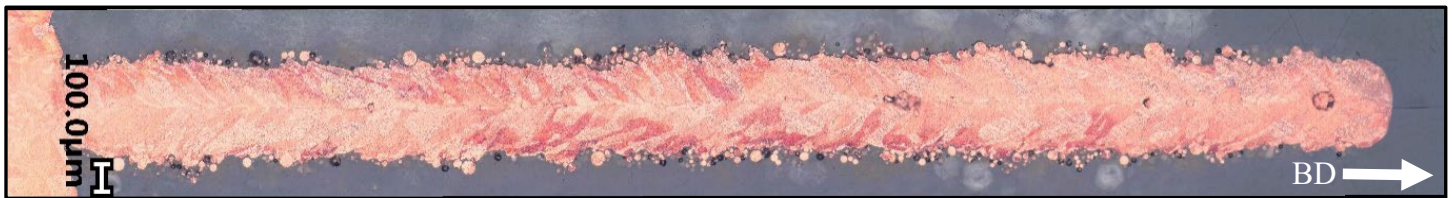

Figure 5: Polished cross-section of a single track wall built with P=400W and v=600mm/s
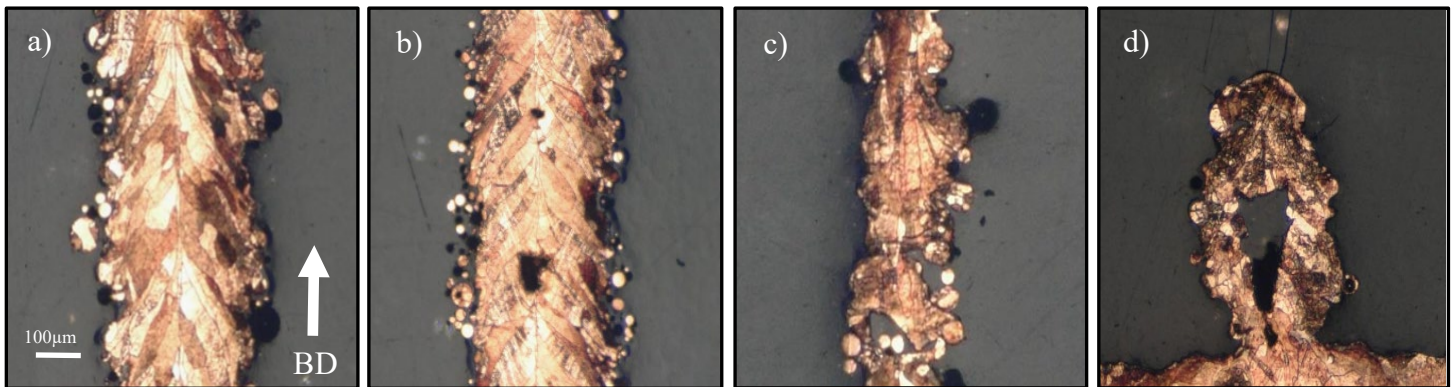

Figure 6: Cross-sections of single track walls showing a) dense walls and formed defects like b) keyhole porosity, c) lack-of-fusion and d) balling

Figure 7 gives an overview of the different regions observed in the produced thin-wall samples for the tested set of parameters. An optimum in the process window can be observed between 600-800mm/s and 400-500W. This region is characterized by dense struts built up of periodically stacked melt pools as shown in Figure 5 and Figure 6.a. The wall thickness is plotted in Figure 8.a. in function of laser power and scan speed. The same data is plotted in Figure 8.b in function of the Line Energy Density (LED). The LED was calculated for every parameter set as follows:

$$LED = \frac{P}{v}$$

Finally, the depth of the melt pool was measured in the processing window. Here, a significant decrease in meltpool depth is measured of $\pm70\mu m$.
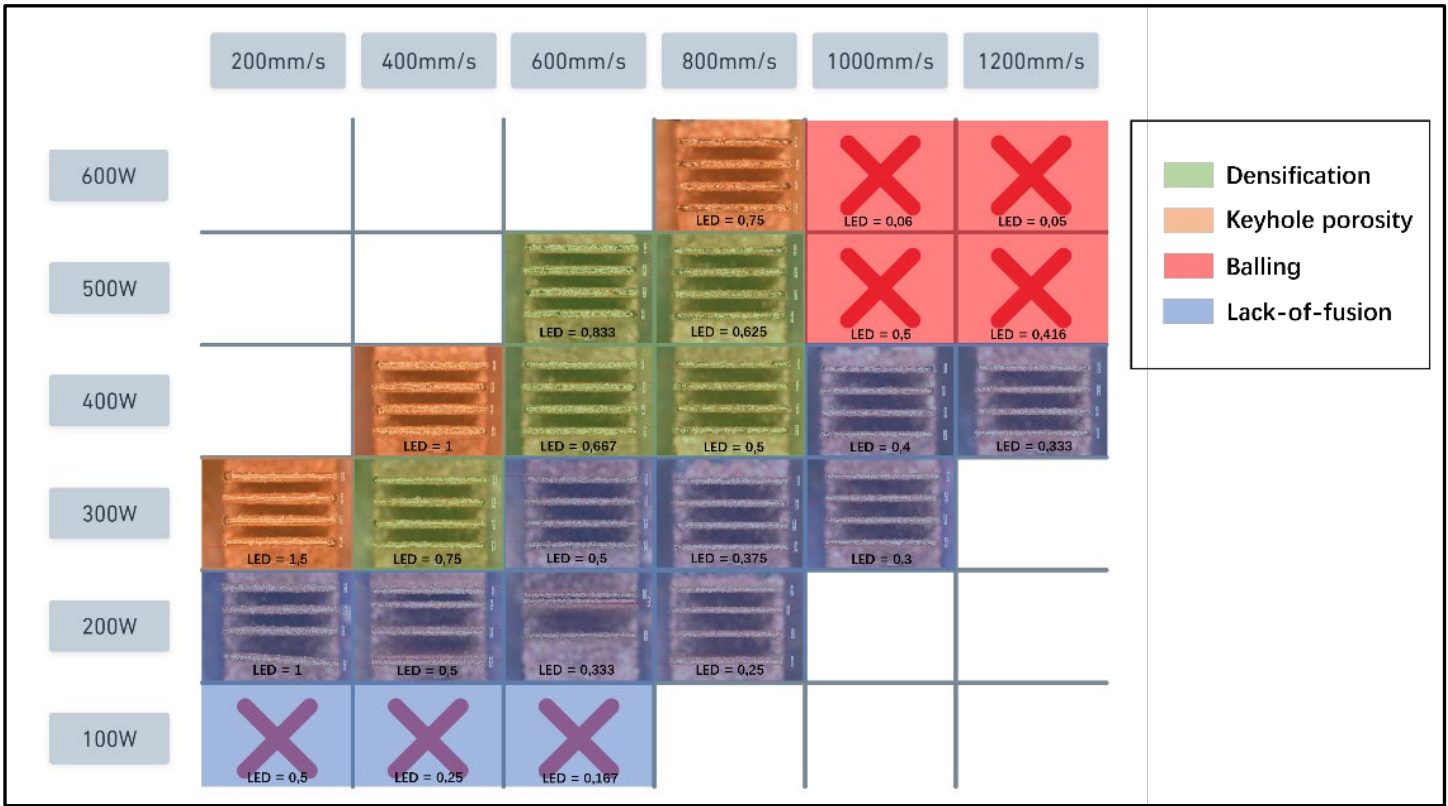
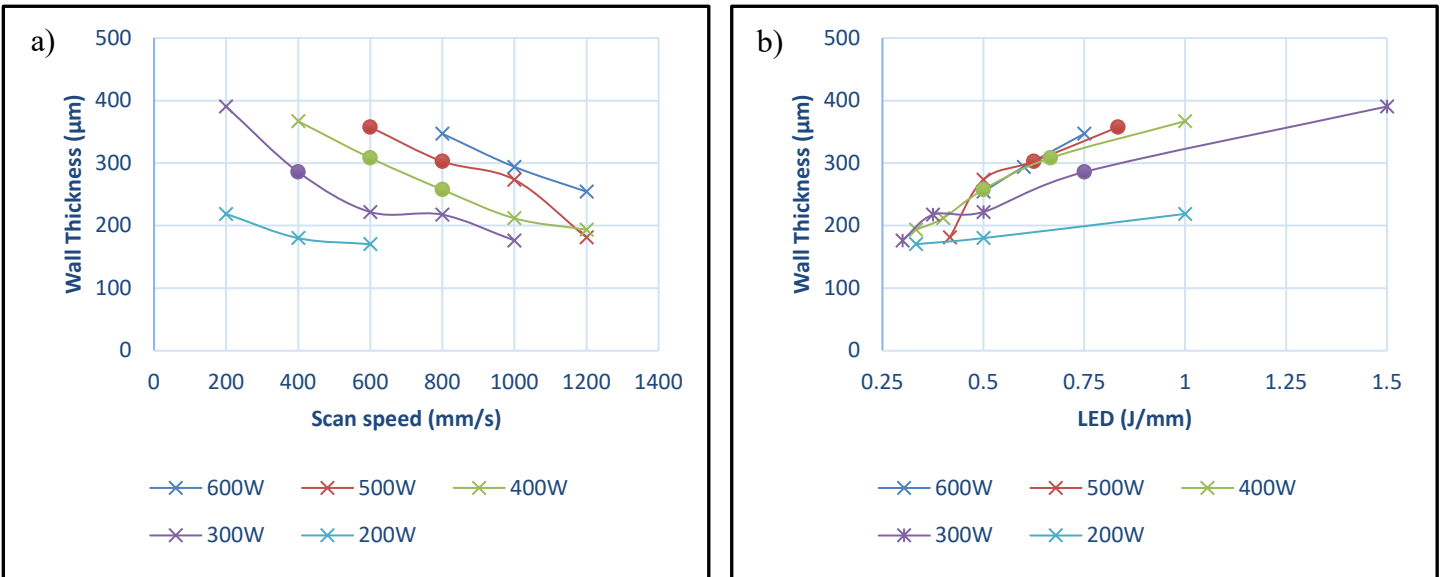*Figure 7: Experimentally obtained process window based on observed defects in cross-sections in single track walls.*

Figure 8: Wall thickness of single track walls in function of a) laser power and scan speed and b) line energy density.

4.2. Inclined thin walls

Within the lattice production framework, the reduction in melt pool depth in single-scan walls that was measured could offer an advantage by enabling the creation of overhangs and inclined surfaces with minimal dross formation. To verify this, thin walls were built under an angle of 80°, 70°, and 60° with respect to the baseplate as shown in Figure 9.a. This initial experiment showed that parameters in the process window lead to dense struts with minimal defects even when produced under an angle. Note that the meltpool in the 60° sample, shown in Figure 9.b., appears to be asymmetrical compared to the 90° samples.
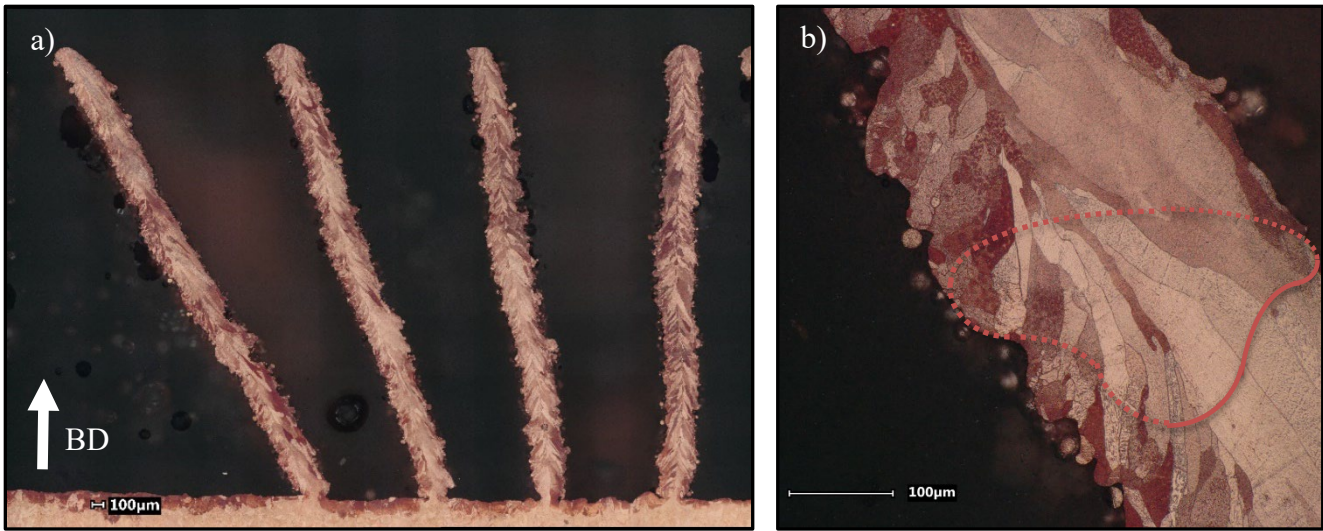
Figure 9: a) Thin wall samples build under 60°,70°,80° and 90° w.r.t. the buildplate, produced with P=400W & v=600mm/s. b) High magnification image of the meltpool in the 60° sample.

4.3. Denudation and thermal isolation and its effect on melt pool size

The experiments mentioned above indicate a significant difference between the melt pool size and shape in bulk, thin wall samples and inclined walls. Figure 10 provides a comparison between the melt pools of bulk samples (a-b-c) and thin wall samples (d-e-f) manufactured with 500W and 600mm/s. In case of the thin wall, the melt pool is consistently wider and less deep compared to the bulk sample. This difference can be explained by the size of the denudation zone and the thermal isolation of the melt pool.

Denudation is defined as the displacement of powder towards the melt pool as a result of a rapidly expanding vapor jet formed above the melt pool. Matthews et al. [8] reported that the denudation zone for Ti64 and 316L SS grows for increasing energy densities in single line scans. Kaserer et al. [9] studied the effect of ambient pressure on the denudation zone size in Ti64 and 316L SS. Both concluded that the denudation zone width under 1atm reached around 400µm. As OF-Cu is preferably processed in keyhole mode, one can assume a denudation zone that grows even larger than 400µm. As literature on this topic is scarce, future measurements are required to quantify the actual denudation zone dimensions for OF-Cu.
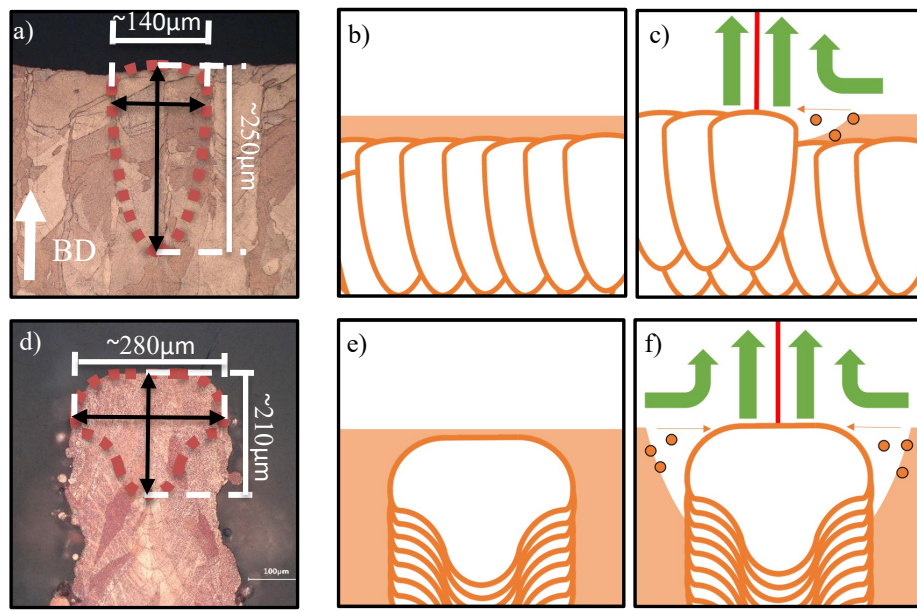

Figure 10: Comparison of the melt pool formation and dimensions in a) bulk samples and d) thin wall samples manufactured with P=500W and v=600mm/s. b&c) The denudation zone in bulk samples. e&f) The denudation zone in thin wall samples.

It is believed that the volume of the denudation zone is the cause for the change in size and shape of the melt pool. In bulk samples the denudation zone is limited to one side and by the layer height (30μm) as shown in figure 10.c. In thin-walled samples, powder is accumulated at both sides of the melt pool. Additionally, the depth of the denudation zone is not limited by the layer height. It can be assumed that the widening of the melt pool can be attributed to two factors: a larger denudation zone and reduced effectiveness in heat dissipation from the pool. Evidence for this statement can be found in the first layers of the produced thin walls as shown in Figure 9.a. and Figure 11. Over these first layers the depth of the denudation zone grows. This clearly reflects in the thickness of the melt pool, and subsequently the thickness of the wall itself, near the baseplate.

Similarly, the inclined wall experiments show the effect of the denudation zone and thermal isolation on the melt pool size. In Figure 9.b. a clear difference is observed in the melt pool when comparing the left (i.e. thermally isolated) and right side (thermally non-isolated) of the melt pool. Again, thermal isolation zones in the melt pool lead to an increase in the melt pool dimensions.
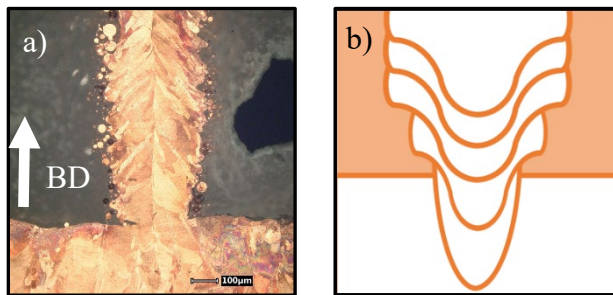

Figure 11: Melt pool behavior during transition from bulk to thin wall

4.4. Strut optimization

Conclusions made from the thin walls studied in the last section are relevant when envisioning strip-fins or surface based lattices such as TPMS structures. However, pin-fin and strut-based lattices are widely studied geometries as well. In this section the melt pool behavior in small struts is analyzed. Vertical struts were produced by scanning small contour-scans ranging from 10μm to 100μm in diameter. The size of the contour is not directly affecting the outside diameter, but is mainly affecting the length of laser-melt pool interaction. If our conclusions from the previous section are correct, one could assume that the denudation zone volume increases even more as powder is attracted from all directions.
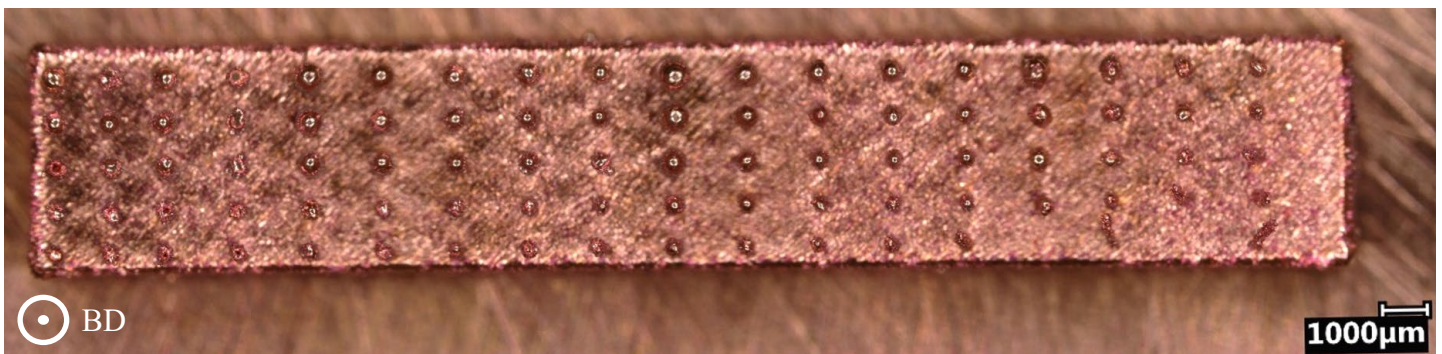

Figure 12: Top-view of struts manufactured by small contours (100μm,75μm,50μm,25μm,10μm) built with parameters ranging from 300W<P<600W & 200mm/s<v<1200mm/s.

The measured thicknesses are summarized in Figure 13. The effect of the scanned diameter on the final strut thickness is shown in Figure 13.a. Smaller struts, and thus shorter laser-melt pool interactions, lead to smaller strut diameters. However, the smallest struts (25μm&10μm scan diameter) showed clear signs of lack-of-fusion. When comparing the strut diameter (full line) with the thin wall thickness (dashed line), as shown in Figure 13.b.,

it is observed that the strut melt pool is consistently larger. Further analysis of the melt pool is needed to construct a process window for struts.
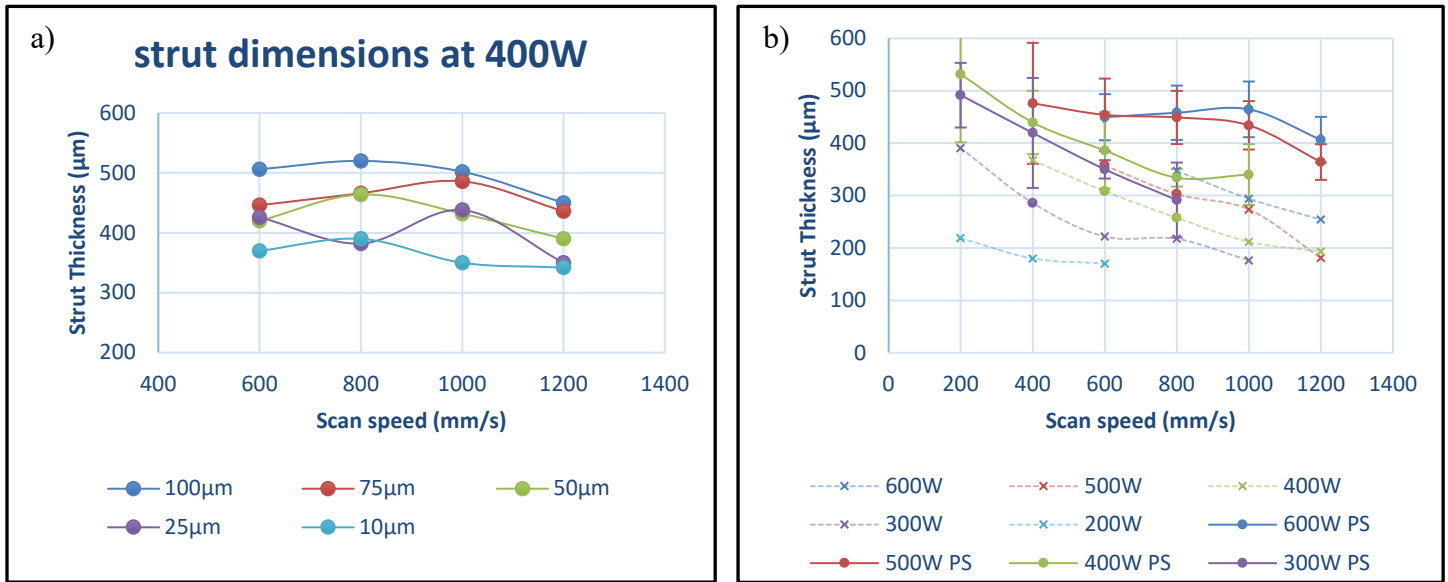

Figure 13: a) A graph showing the effect of the contour diameter on the strut thickness for a set power (400W) and varying scan speed. b) Comparison of the wall thickness (dashed line) and strut thickness (full line) in function of the process parameters.

5. Conclusion

Laser Powder Bed Fusion with a 1kW fiber laser has been proven effective in manufacturing bulk, thin wall and strut samples. Process windows were constructed for OF-Cu LPBF at different baseplate preheating temperatures. Baseplate preheating of T=300°C showed significant improvements in process stability of bulk samples. Samples built with preheating, P=540W and v=790mm/s resulted in high density (99.7%). The melt pools dimensions at 300°C preheating were compared to measurements reported by Jadhav et al. [4] which showed a slight increase in melt pool depth.

Through cross-sectional analysis of single-track walls, significant changes in the size and shape of the melt pool were observed. An increase in width of 80% and decrease in depth of 25% was measured for stable melt pools. This evolution of a bulk to single track melt pool lead to necking in the first layers of the single wall. The alteration of the melt pools is thought to be attributed to the volume of the denudation zone and thermal isolation. As more powder is found in proximity to the melt pool and heat removal is less efficient, as is the case for thin walls, it grows in width. The thinnest fully dense walls were built using preheating, P=400W and v=800mm/s and measured ≈250µm. Finally, struts were manufactured by stacking small contours that again lead to a small increase in melt pool dimension.

6. Acknowledgements

References

1) Yegyan Kumar, A., Wang, J., Bai, Y., Huxtable, S. T., & Williams, C. B. (2019). Impacts of process-induced porosity on material properties of copper made by binder jetting additive manufacturing. *Materials and Design*, *182*, 108001. https://doi.org/10.1016/j.matdes.2019.108001

2) Thomas, A., Fribourg, G., Blandin, J. J., Lhuissier, P., Dendievel, R., & Martin, G. (2021). Effect of the build orientation on mechanical and electrical properties of pure Cu fabricated by E-PBF. *Additive Manufacturing*, *48*, 1–28. https://doi.org/10.1016/j.addma.2021.102393

3) Qu, S., Ding, J., Fu, J., Fu, M., Zhang, B., & Song, X. (2021). High-precision laser powder bed fusion processing of pure copper. *Additive Manufacturing*, *48*(PA), 102417. https://doi.org/10.1016/j.addma.2021.102417

4) Jadhav, S. D., Goossens, L. R., Kinds, Y., Hooreweder, B. Van, & Vanmeensel, K. (2021). Laser-based powder bed fusion additive manufacturing of pure copper. *Additive Manufacturing*, *42*(February). https://doi.org/10.1016/j.addma.2021.101990

5) Unitek Miyachi Corporation. (2003). *in Nd : YAG Laser Welding*. http://www.miyachieurope.com/cmdata/documents/laser-welding-fundamentals.pdf

6) Tolochko, N. K., Laoui, T., Khlopkov, Y. V., Mozzharov, S. E., Titov, V. I., & Ignatiev, M. B. (2000). Absorptance of powder materials suitable for laser sintering. *Rapid Prototyping Journal*, *6*(3), 155–160. https://doi.org/10.1108/13552540010337029

7) Kadivar, M., Tormey, D., & McGranaghan, G. (2021). A review on turbulent flow over rough surfaces: Fundamentals and theories. *International Journal of Thermofluids*, *10*(March), 100077. https://doi.org/10.1016/j.ijft.2021.100077

8) Matthews, M. J., Guss, G., Khairallah, S. A., Rubenchik, A. M., Depond, P. J., & King, W. E. (2016). Denudation of metal powder layers in laser powder bed fusion processes. *Acta Materialia*, *114*, 33–42. https://doi.org/10.1016/j.actamat.2016.05.017

9) Kaserer, L., Bergmueller, S., Braun, J., & Leichtfried, G. (2020). Vacuum laser powder bed fusion—track consolidation, powder denudation, and future potential. *International Journal of Advanced Manufacturing Technology*, *110*(11–12), 3339–3346. https://doi.org/10.1007/s00170-020-06071-6